Comparison of SOFC and PEM Fuel Cell Hybrid Power Management Strategies for Mobile Robots

Jason B. Siegel, Yuanzhan Wang, and Anna G. Stefanopoulou
Department of Mechanical Engineering
University of Michigan
Ann Arbor Mi 48109, USA
siegeljb@umich.edu

Buz A. McCain
Product Development, Systems Engineering Group
Ballard Power Systems Inc.
Burnaby, BC, Canada V5J 5J8

***Abstract*— Mobile robots for surveillance applications require quiet, high-endurance power sources for their long mission run times. This need cannot be met by batteries alone due to their low energy density or with combustion engines due to noise. A hybrid system combining a high power Lithium ion battery with a high energy density fuel cell (FC) system is ideal for this application. A propane powered 200W solid oxide fuel cell (SOFC) developed by Ultra Electronics is an example of one such system. This fuel cell should be operated at full power to obtain maximum system efficiency or turned off to conserve fuel. This operating strategy with quantized power levels (either on or off) must be paired with a battery to provide the energy to re-start the fuel cell and power the vehicle during turndown periods. We compare the hybridized SOFC system to one with an open cathode Proton Exchange Membrane (PEM) Fuel Cell paired with a battery that allows the PEM FC to load-follow or load-level. The application to military tracked robots for two distinct profiles (realistic driving and scouting) is considered as an example and highlights the need for concurrent power source sizing and power splitting.**

Keywords— Power management, hybrid powertrain, fuel cell, lithium ion battery.

I. Introduction

Mobile robots for surveillance applications require quiet, high-endurance power sources for their long mission run times. This need cannot be met by batteries alone due to their low energy density (180 Wh/Kg, 290 Wh/L), or with combustion engines due to noise. A hybrid system combining a high power lithium ion battery with a high energy density fuel cell system is ideal for this application.

A hybrid power system that combines a battery with a small propane-fueled solid oxide fuel cell (SOFC) for a mobile robot has been simulated using an Ultra Electronics AMI 200 Watt fuel cell and a high energy BB2590 battery pack [1]. The SOFC hybrid system is compared with a 135W micro-PEMFC from Ballard power systems paired with a high power Lithium-Iron-Phosphate (LFP) battery pack. The SOFC power plant has a quantized behavior (1) the fuel cell lacks load-following ability [1] and therefore operates most of the time at a constant power output; (2) each SOFC startup and shutdown event takes several minutes and consumes significant battery power. This SOFC achieves optimum fuel utilization at full load, since the fuel flow rate is constant, and part loading is very inefficient. Therefore it is preferred to operate the FC stack in an on/off manner, however determining when to turn on and off the fuel cell to achieve optimum fuel utilization is not trivial. While the conventional continuously operated hybrid [4]-[7] has been heavily studied, the quantized FC-battery hybrid has not been studied apart from the hybridization with a gas turbine [11]-[12]. New systematic methodologies are needed to get optimum power and endurance from this system.

This paper addresses the power split of two energy dense fuel cell power sources, hybridized with lithium ion batteries. The resulting power splits are compared for two different usage profiles correspond to realistic driving and scouting missions. Fuel cell sizing, dynamic performance (ability to change loads), and efficiency (as a function of output power) have a large impact on the performance and fuel economy of the overall system. The power split and scheduling of shutdowns are investigated via optimization (minimization of fuel consumption) using Dynamic Programming (DP) and a simulation model of various hybridized battery and fuel cell systems.

It is shown that if the peak efficiency point of the fuel cell is larger than the average power demand, then it is optimal to operate either FC in an on-off manner. When the FC peak efficiency point is lower than the average power required (in the case of a PEMFC with lower power rating) then it is optimal to operate the FC continuously. In the case of the SOFC system, there is additional fuel penalty for starting and shutting down the system, which reduces the number of on off switches, forcing the system to run on the battery for longer periods of time in a charge depleting mode. Therefore the thermal limitations and degradation of the battery may be a concern for missions with higher RMS power requirements. For the PEMFC, the efficiency curve is very flat above a certain power level as shown in Figure 7, therefore it would be advantageous to operate in a load following mode [10], subject to constraints on the rate of change in output power [19].

II. System Power and Energy Requirements

The iRobot packbot, which is a tracked robot, is considered for this study. The packbot weighs 11kg without batteries and is typically powered by 2 BB-2590/U lithium ion battery packs which provide more than 4 hours of continuous runtime and up to 10 miles of travel according to the manufacturer. Our goal is to extend the operating time beyond 10 hours, which would require 1130 Wh of energy or roughly 3x the number of

The authors wish to acknowledge the technical and financial support of the Automotive Research Center (ARC) in accordance with Cooperative Agreement W56HZV-14-2-0001 U.S. Army Tank Automotive Research, Development and Engineering Center (TARDEC) in Warren, MI.

978-1-4673-7637-2/15/$31.00 ©2015 IEEE

batteries. The specification for the BB2590U battery are shown in Table II. The fuel efficiencies will be evaluated using two different load profiles. The first load profile shown in Fig. 1 captures real-world driving measured with an instrumented packbot [3].

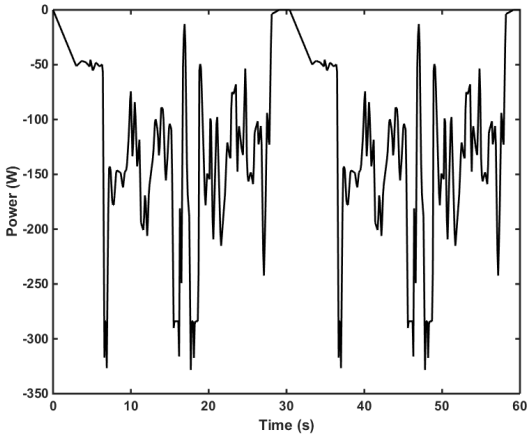

Figure 1: Typical robot power profile [3].

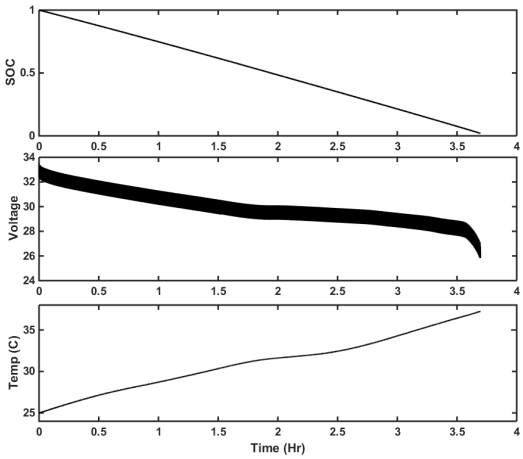

Figure 2: Battery state of charge, voltage and temperature for the repeated discharge power profile shown in Fig. 1 when the robot is operated using only two BB-2590 modules.

For this cycle the average power draw is 113 W, the maximum power draw is 328 W and the standard deviation is 80 W. The second profile is for a scouting/area coverage cycle reported in [2] which consists of long durations of constant power operation followed by higher power turning maneuvers. The scouting profile has an average power draw of 76 W, the maximum power draw of 164 W and the standard deviation of 14 W. The average power of the driving cycle is above the selected Ballard micro-FC peak efficiency point and the scouting profile is below.

III. System Architecutre

There are two common options for hybridizing the fuel cell with a battery either direct parallel connection of battery and fuel cell with a diode (to prevent back feeding current into the fuel cell), and use of DC/DC converter with the load either connected to the FC or battery as shown in Fig. 3. Other variations combining the above schemes may also be considered such as utilizing a small buck converter for optimum efficiency point operation with direct connection for high power (thus enabling operation with smaller DC/DC converter rating) [20],[21].

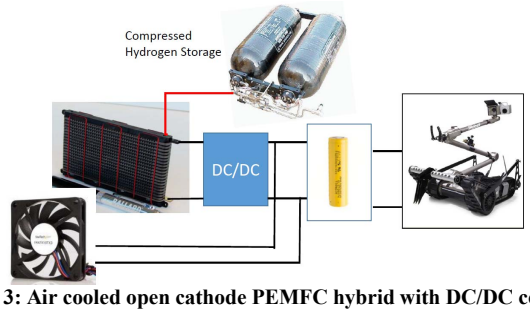

Figure 3: Air cooled open cathode PEMFC hybrid with DC/DC converter and high power lithium ion battery.

A DC/DC is connected between the battery and PEM fuel cell as shown in Fig. 3. The SOFC has the same architecture. We also assume that the fuel cell auxiliaries, fans and purge valves powered by the battery pack to avoid issues of directly connecting unregulated loads to the fuel cell [18]. In the future we plan to expand the sizing analysis to consider the direct parallel connection of energy devices as in [20] to eliminate the DC/DC converter and enable cost reduction in the PEMFC hybrid system.

IV. Component Modeling and Optimization

A. Battery

The standard Packbot configuration uses 2 BB2590U packs storing 6.8 Ah each. Inside each ruggedized plastic container are 24 18650 cells packaged with electronics to perform battery management, protection, and cell balancing. The cells are connected 3 each in parallel and then 8 in series (3P8S) arrangement. Due to the packaging and sealed plastic waterproof container there is limited heat rejection from the battery pack and temperature rise during operation is a concern for battery only operation [13], as shown by the 10 degree temperature rise in a few hours in Fig. 2.

The SOFC is paired with a single low power high energy density BB-2590 pack because the SOFC can also provide high power but has extended transition phases requiring significant energy from the battery. The PEMFC hybrid system on the other hand has relatively low power (compared to robot peak power) so we consider a sized pack of A123 18650 high power cells with 1.1 Ah capacity. The number of serial and parallel connected cells is tailored to the application to minimize the battery weight while providing the peak power requirement. We chose a 1P10S arrangement to be comparable to the nominal voltage (28V) and power capability of the BB pack as in Table III.

Both Lithium-ion batteries can be modeled using a 4-state electro-thermal model of the cylindrical cell [16]. This model consists of a single R-C equivalent circuit and state of charge plus two thermal states. For the purpose of DP the battery model can be further reduced to 2 states (V_1 and SOC), when the battery temperature is well regulated, with little loss in fidelity. The reduced model consists of a single R-C equivalent circuit with series resistance and state of charge, appropriate for the low C-rate (<1C) operation of the battery [14].

$$P_{batt} = P_{dmd} - P_{aux} - P_{fc} = (V_{OCV}(SOC) - V_1 - I_{batt}R_{int})I_{batt} \quad (1)$$

$$\frac{dSOC}{dt} = -\frac{I_{batt}}{Q_{cap}} \quad (2)$$

$$\frac{dV_1}{dt} = \frac{I_{batt}}{C_1} - \frac{V_1}{C_1 R_1} \quad (3)$$

$$\frac{dT_{batt}}{dt} = h \cdot A \cdot (T_{batt} - T_{amb}) + Q_{gen}(P_{batt}, V_1, SOC) \quad (4)$$

The open circuit voltage V_{OCV} is a function of the battery SOC, and the battery resistances R_1 and R_{int} depend strongly on temperature when cold, but remain relatively constant for the temperature range of interest here.

To predict capacity fade of the battery, a semi-empirical model from [25] is adopted. This model is established by using a power law equation to relate charge throughput with capacity fade and an Arrhenius correlation to account for temperature effects.

$$Q_{loss} = B\int \exp\left[\frac{-31700Q_{cap} + 370.3|I_{batt}|}{Q_{cap} R T_{batt}}\right](|I_{batt}|dt)^{0.55} \quad (5)$$

The parameters of the capacity fade model are experimentally derived in [25] and [27] for LFP and BB cells respectively. Parameterization for the LFP electrothermal model is given in [15] while [16] contains all information for parameterizing the BB model.

B. *Solid Oxide Fuel Cell system*

The Ultra-AMI SOFC runs on commercial propane cylinders. A 1 L cylinder contains about 0.5kg of propane. The fuel is consumed at a constant flow rate of 0.102 kg/hr, regardless of electrical load, to meet the power demands of the auxiliaries and maintain the temperature. SOFCs are very sensitive to thermal shock due to their ceramic materials and therefore the temperature must be well controlled [11]-[12]. Due to the low efficiency of the SOFC at part loading it is preferable to shut down the system rather than idle it. However, the SOFC has a 16 minute startup procedure which requires 6.5 Wh of energy to heat up the stack before power can be generated as explained in [1]. Similarly the shutdown procedure requires 5.3 Wh of energy and takes 18 minutes. Therefore the SOFC must be paired with a relatively large energy storage battery and proper scheduling of the shutdowns for the fuel cell is critical to achieve optimum system efficiency. For this study the SOFC is paired with a single BB-2590 battery pack.

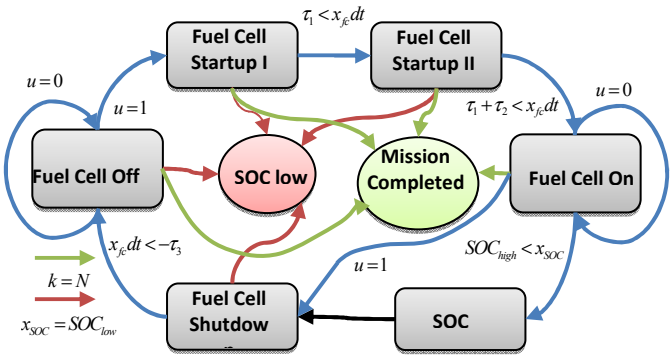

Figure 4: SOFC startup flow diagram [1].

The SOFC is modelled by four discrete phases, on, off, startup and shutdown, the latter two of which also consume energy. The startup phase is further divided into two sub-phases, the second of which draws less electrical power than the first but consumes same rate of fuel as normal operation [1]. A flow chart showing how this hybrid system works is shown in Figure 4.

Dynamic Programming is used to determine the control strategy that minimizes fuel consumption according to the following cost function.

$$J = \sum_{k=1}^{N} W_{H_2}(k) \quad (6)$$

Where W_{H_2} is the fuel consumption rate (0.102 kg/hr when on or at startup phase II, and zero otherwise). The state x_1 indicates the duration of time the fuel cell is in each startup or shutdown phase while x_2 denotes battery state of charge. A 10s time step, dt, was used and the power profiles were averaged over the same interval as shown in Figure 5.

$$x_1(k) = fc(k) \in \left[-\frac{\tau_3}{dt}, \frac{\tau_1+\tau_2}{dt}\right] \quad (7)$$

$$x_2(k) = SOC(k) \in [SOC_{low}, SOC_{high}] \quad (8)$$

The battery state V_1 can be removed in the DP analysis for the SOFC case, since the C-rate operation of the battery is low (<2C) and the SOC range is constrained below 0.8. In the case where the battery upper voltage limit is a concern, such as constant voltage charging, the V_1 state should be included.

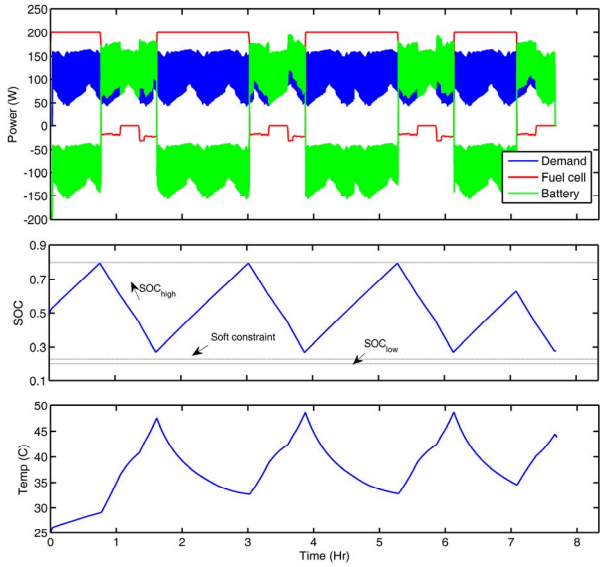

Figure 5: Realistic driving cycle for SOFC hybrid showing power split, battery SOC and battery temperature.

If the fuel cell is fully loaded when on, so that it is used most efficiently, then the control strategy is simply a series of on/off commands. The resulting SOC trajectory exhibits a cyclic and charge/discharge behavior as in Figure 5 rather the classical monotonically decreasing one. Charge depletion is a natural result of fuel saving oriented DP because it will always try to deplete energy stored in battery to save fuel for a given

power profile [23]. The scouting cycle shows a similar result except for slope of SOC trajectory because of different power demands. Since the SOFC hybrid uses only 1 BB-Pack temperature rise is an issue as shown in Figure 5. The average battery current during charging is lower than the discharging portion of the cycle, when traction power is split between the battery and FC, therefore the battery temperature decreases.

C. PEM Fuel Cell system

The system architecture for the PEMFC hybrid power plant is shown in Fig. 3. A high pressure compressed hydrogen storage tank is used for its high gravimetric energy density. The tank supplies low pressure (50 kPa) regulated fuel to the stack. A 3L hydrogen storage tank at 30 MPa was chosen to provide the energy storage needed for 10 hour operating time (approximately 75g of H_2).

The cathode is open and excess air, driven by a fan, flows over the stack to provide adequate cooling and excess oxygen for the reaction. Each 45W stack requires 100 standard liters per minute of air for cooling at rated power, roughly 100x the amount required for the reaction at peak power. This fan represents the largest parasitic loss to the fuel cell [24]. We assume the fan draws a constant value of 10W from the battery pack so that the proposed PEMFC will have a maximum net power of 125W. The DC/DC converter regulates power drawn from the fuel cell. We assume startup and shutdown has no energy penalty, however purging of the water and nitrogen from the dead-ended anode is required to prevent degradation [17].

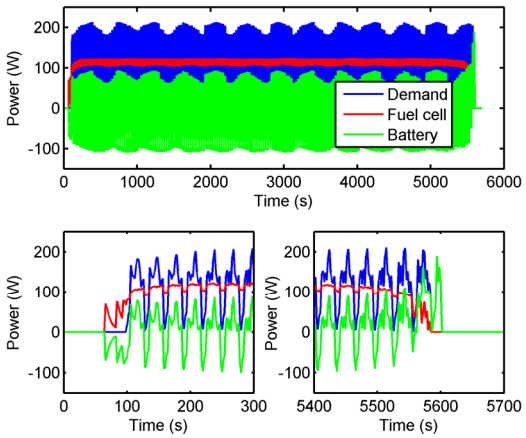

Figure 6: Driving cycle with on SOC deviation penalty.

By limiting the rate of change in power drawn from the fuel cell a static model for the fuel cell can be used [7]-[9], [19]. The fuel cell terminal voltage as a function of current can be expressed by the following empirical relationship

$$V = E_{rev}^{0} + \frac{RT}{nF}\ln\left(\frac{p_{H_2} p_{O_2}^{0.5}}{p_{H_2O}}\right) - \frac{RT}{\alpha F}\sinh^{-1}\left(\frac{i_{loss}+i}{2i_{0,c}}\right) - i\left(\mathrm{R}_{ion}\right) + B_c \ln\left(1-\frac{i}{i_{\max,c}}\right), \quad (9)$$

where i is the current drawn from the cell. The remaining constants have been adapted from [22]. The fuel consumption rate is given by

$$w_{H_2} = \frac{i}{nF} M_{H_2} \quad (10)$$

where M_{H_2} is the molar mass of hydrogen, n=2 and F is Faradays constant. The efficiency can then be defined as the output power ($P = i \cdot V$) divided by the power of the input fuel using the lower heating value of fuel as follows,

$$\eta = P / \left(w_{H_2} \cdot LHV_{H_2} \cdot 3600\right) \quad (11)$$

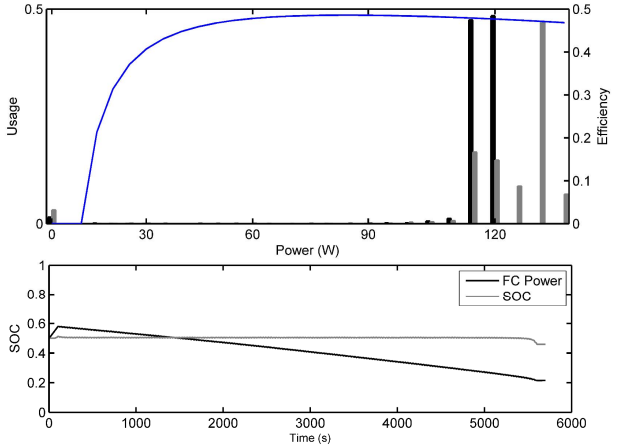

Figure 7: FC utilization and system efficiency vs power (top) Battery SOC (bottom) for the realistic drive cycle comparing the penalty on SOC deviation and deviation from the FC peak efficiency point.

For system level analysis, dynamics of the fan and the fuel cell are neglected. A charge sustaining strategy is first considered by constructing a cost function for DP as follows,

$$J = \sum_{k=1}^{N} \left(\beta W_{H_2}(k) + \alpha (SOC_{ref} - SOC(k))^2\right) \quad (12)$$

This cost function penalizes both the deviation in state of charge and the total fuel consumption. The weights α and β are set so that when $\Delta SOC = 0.1$ and $W_{H_2} = W_{H_2}(I_{max}) = 2.262$ [mg/s], $\alpha(\Delta SOC)^2 = \beta W_{H_2} = 1/2$, i.e., each variable contributes equally to the cost. The time step dt is set to 2 seconds and power profiles are averaged over the 2 seconds as shown in Figure 6. The two dynamic state equations for DP correspond to the battery model;

$$x_1(k) = SOC(k) = SOC(k-1) - \frac{I(k)}{Q_{cap}} dt \quad (13)$$

$$x_2(k) = V_1(k) = V_1(k-1) + \left(\frac{I(k)}{C_1} - \frac{V_1(k-1)}{C_1 R_1}\right) dt \quad (14)$$

In the optimal trajectory, the SOC is regulated around the reference point 50% SOC except at starting up and final stages as shown in by the gray line in the bottom subplot of Figure 7. The fuel cell works above 120W gross power as shown by the gray bars in the upper frequency plot of Figure 7. This is close to the average power demand of the driving mission, and above the FC peak efficiency point. A similar result can be seen in the gray lines of Figure 8, for the scouting mission which frequently uses 80W fuel cell power at near peak efficiency.

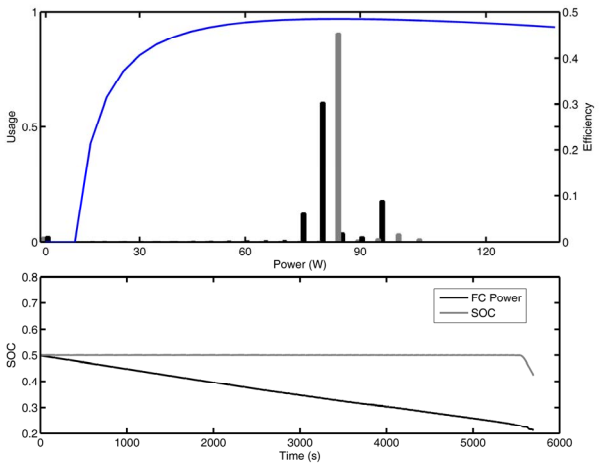

Figure 8: FC utilization and efficiency vs power (top) Battery SOC (bottom) for the scouting cycle.

Next we consider a charge depletion strategy with penalty on deviation from ideal working points (quantized power level) of the fuel cell. We select the reference H_2 flow rate from the FC peak efficiency point (85W) and construct the following cost function,

$$J = \sum_{k=1}^{N} (\beta W_{H_2}(k) + \alpha (W_{H_2,ref} - W_{H_2}(k)))^2 \qquad (15)$$

The fuel cell now works at a narrower range for the realistic driving cycle, shown in Figure 7 where the black lines in the upper subplot are more tightly grouped, as compared to penalizing SOC deviation shown in grey. However for the scouting mission the optimal profile for this cost function has higher and lower operating points than previously. The scouting mission shown in Fig. 8 has lower average power demand, and hence the FC operating points are centered about the peak efficiency. Both Fig 7. and Fig. 8 show a charge depleting behavior of the battery (black line) for this cost function, with a lower average FC power. In the case of the scouting mission we also have some zero power operating conditions where the PEMFC is shut down allowing the system to achieve a higher efficiency. Therefore it is possible to optimize the hybrid system by with a quantized PEMFC, with the power levels of determined by the fuel cell efficiency curve and allowable SOC deviation.

TABLE I. DP RESULTS FOR BATTERY FADE AND FUEL CONSUMPTION

Profile 1/2 Drive/Scout	Battery Capacity Fade (%)	Equiv. Fuel Consumption (g)	Battery Peak Temperature (C)
Battery SOC	0.33 / 0.11	11.40 / 7.62	28.6 / 26.2
FC Eff	0.38 / 0.13	11.39 / 7.60	30.9 / 27.1

It can be seen from the table above that for the driving cycle, when there is penalty on SOC or selected working point, the battery pack fades faster because the fuel cell works more on a load-leveling basis and the dynamic cycle will hence have a larger effect on it. It is also obvious that battery fades at a much slower rate when executing the second profile because the profile is in itself quantized (long periods of constant power demand) and the battery suffers less from varying power demand. Fuel cell and battery temperatures are not a major issue in these cases but could be for missions with higher RMS powers.

D. Comparison

The SOFC hybrid system achieves an efficiency of 15.4 % for the driving cycle and 14.8 % for the scouting mission (when the lower and higher SOC bounds are set to 0.2 and 0.8 respectively). This result is lower than the 19% efficiency predicted in Table III for steady operation due to parasitic losses associated with the multiple startup/shutdown sequences. The corresponding efficiency values achieved by PEMFC system are 47.2% and 48.5% respectively, both of which are much higher than those of SOFC system. Nevertheless, the SOFC system has its own advantages as it uses swappable military standard bb2590 battery cells and operates on readily available and easy to refill compressed Propane cylinders.

V. CONCLUSIONS

For the base case sizing we choose a PEMFC capable of delivering the average power draw of 113W at the nominal voltage of 28V. Therefore 3 of the PEMFC stacks (11.2V each at 45W) are chosen to be put in series for a total capability of 135W of power generation. The fuel cell stack is connected to a series string of 10 A123 18650 cells through a DC/DC buck converter which allows for control of the power taken from the stack. The load is directly connected to the battery as shown in Fig. 3.

Table II shows the energy density for the components of the AMI/BB hybrid and the PEMFC/A123 battery systems. The combined energy density of the hybridized SOFC system is 263 [Wh/kg] and 122 [Wh/L] which is much lower than the proposed PEMFC based hybrid system which has energy densities of 516 [Wh/kg] and 258 [Wh/L]. The SOFC configuration presents new power management challenges due to its quantized power operation and long shut-down and start-up phases. This quantized operation presents also potential opportunities in designing a PEM balance of plant (BOP) with on-off fans and tailored DC/DC converters for lower cost. In the future we will develop the PEMFC+A123 high power battery hybrid powertrain and we will assess the real system efficiency and range through simulations as a function of battery and stack size.

TABLE II. COMPARISON OF SYSTEM PROPERTEIS

System Properties	**AMI SOFC + 1 Propane tank and 1x BB-2590**	**Micro PEMFC + H2 tank with 10S1P A123 18650**
system volume [L]	11.5	5.35
system weight [kg]	6.3	2.67
Usable Energy [Kwh]	1.32	1.38
Energy density [Wh/kg]	263	516
Energy density [Wh/L]	122	258
Projected runtime [h]	11.7	12.3

ACKNOWLEDGMENT

The authors would like to acknowledge support from Yi Ding, Matthew Castanier, and Kevin Centeck at TARDEC for their

insight and advice about the mobile robot application and power requirements.

REFERENCES

[1] J. Broderick, J. Hartner, D. Tilbury, and E. Atkins, "Modeling and simulation of an unmanned ground vehicle power system," SPIE Defense+ Security, pp. 908406-908406-10, 2014

[2] J. Broderick, D. Tilbury, and E. Atkins, "Experimental analysis of packbot energy usage," Journal of Field Robotics, March 2014.

[3] K. Boice, A. Leo, J. Lee, J. Paulson Jr., M. Skalny, and T. Valascho, "Baseline field testing of BB-2590 lithium-ion batteries using an iRobot Fastac 510 robot," tech. rep., TARDEC, 2010.

[4] J. Liu and H. Peng, "Modeling and Control of a Power-Split Hybrid Vehicle," IEEE Transactions on Control Systems Technology, vol. 16, no. 6, pp.1242-1251, 2008

[5] C.C. Lin, H. Peng, J. W. Grizzle, and J. Kang, "Power Management Strategy for a Parallel Hybrid Electric Truck," IEEE Transactions on Control Systems Technology, vol. 11, pp. 839-849, November 2003

[6] L. Guzzella and A. Sciarretta, "Vehicle Propulsion Systems - Introduction to Modeling and Optimization", 3rd. Ed., 2013, Springer

[7] J. T. Pukrushpan, A. G. Stefanopoulou, and H. Peng, "Control of Fuel Cell Power Systems - Principles, Modeling, Analysis and Feedback Design," 2004, Springer

[8] A. Vahidi, A. G. Stefanopoulou, and H. Peng, "Current Management in a Hybrid Fuel Cell Power System: A Model Predictive Control approach," IEEE Transactions on Control Systems Technology, vol. 14, pp. 1047-1057, 2006

[9] A. Vahidi, I. Kolmanovsky, and A. G. Stefanopoulou, "Constraint Handling in a Fuel Cell System: A Fast Reference Governor Approach," IEEE Transactions on Control Systems Technology, vol. 15, pp. 86-98, 2007

[10] O. Sundstrom and A. G. Stefanopoulou, "Optimal power split in fuel cell hybrid electric vehicle with different battery sizes, drive cycles, and objectives," In Proc. IEEE Computer Aided Control System Design IEEE International Conference on Control Applications IEEE International Symposium on Intelligent Control, pp. 1681-1688, 4-6 Oct. 2006

[11] V. Tsourapas, J. Sun, and A. Stefanopoulou, "Control oriented analysis of a hybrid solid oxide fuel cell and gas turbine system," Journal of Fuel Cell Science and Technology, vol. 6, no. 4, 041008, 2009

[12] S.R. Oh, J. Sun, H. Dobbs, and J. King, "Model Predictive Control for Power and Thermal Management of an Integrated Solid Oxide Fuel Cell and Turbocharger System," IEEE Transactions on Control Systems Technology, vol.22, no.3, pp.911-920, 2014

[13] T. Ersal, Y. Kim, J. Broderick, T. Guo, A. Sadrpour, A. Stefanopoulou, J. B. Siegel, D. Tilbury, E. Atkins, H. Peng, J. Jin and A. G. Ulsoy, "Keeping ground robots on the move through battery and mission management," ASME Dynamic Systems and Control Magazine, vol. 2, no. 2, pp. 1-6, 2014

[14] Y. Li, and D. Anderson. "Estimation and Compensation of Battery Measurement and Asynchronous Biases". US Patent Application no 2015/0158395.

[15] X. Lin, H. E. Perez, S. Mohan, J. B. Siegel, A. G. Stefanopoulou, Y. Ding and M.atthew P. Castanier. "A Lumped-Parameter Electro-thermal Model for Cylindrical Batteries", Vol. 257, pp. 1-11, Journal of Power Sources, 2014.

[16] Y. Kim, S. Mohan, J.B. Siegel, A.G. Stefanopoulou, and Y Ding, "The Estimation of Temperature Distribution in Cylindrical Battery Cells under Unknown Cooling Conditions", IEEE Transactions on Control Systems Technology, doi: 10.1109/TCST.2014.2309492

[17] T. Matsuura, J. Chen, J. Siegel, and A. Stefanopoulou, "Degradation phenomena in PEM fuel cell with dead-ended anode," International Journal of Hydrogen Energy, vol. 38, pp. 11346-11356, 2013.

[18] K. Suh and A. G. Stefanopoulou. "Performance Limitations of Air Flow Control in Power-Autonomous Fuel Cell Systems." IEEE Transactions on Control Systems Technology, vol. 15, no. 3, pp. 465-473, May 2007.

[19] O. Sundstrom, A. G. Stefanopoulou, "Optimum Battery Size for Fuel Cell Hybrid Electric Vehicle, Part I," ASME Journal of Fuel Cell Science and Technology, vol. 4, pp. 167-175, May 2007.

[20] Akira Nishizawa, Josef Kallo, Olivier Garrot, Jörg Weiss-Ungethüm, "Fuel cell and Li-ion battery direct hybridization system for aircraft applications," Journal of Power Sources, vol. 222, pp. 294-300, January 2013.

[21] Jih-Sheng Lai; Nelson, D.J., "Energy management power converters in hybrid electric and fuel cell vehicles," Proceedings of the IEEE , vol.95, no.4, pp.766-777, April 2007.

[22] M. M. Mench, *Fuel Cell Engines.* Hoboken, NJ. Wiley, 2008.

[23] Bubna, Piyush, et al. "Prediction-based optimal power management in a fuel cell/battery plug-in hybrid vehicle." Journal of Power Sources 195.19 (2010): 6699-6708.

[24] Sasmito, A. P., et al. "Computational study of forced air-convection in open-cathode polymer electrolyte fuel cell stacks." Journal of Power Sources 195.17 (2010): 5550-5563.

[25] Wang, John, et al. "Cycle-life model for graphite-LiFePO 4 cells." Journal of Power Sources 196.8 (2011): 3942-3948.

[26] Müller, Eric A., and Anna G. Stefanopoulou. "Analysis, modeling, and validation for the thermal dynamics of a polymer electrolyte membrane fuel cell system." Journal of fuel cell science and technology 3.2 (2006): 99-110

[27] Wang, John, et al. "Degradation of lithium ion batteries employing graphite negatives and nickel–cobalt–manganese oxide+ spinel manganese oxide positives: Part 1, aging mechanisms and life estimation." Journal of Power Sources 269 (2014): 937-948.

TABLE III. COMPARISON OF ENERGY STORAGE COMPONENTS

Component Properties	**BB-2590U**	**A123 186501.1 Ah**	**AMI SOFC**	**Micro PEMFC**	**Propane**	**3L 30MPa H_2**
Power [W]	288	660 (10S1P pack)	245	135 (3x stacks)	--	--
Voltage [V]	28.8 (33.6 Max/24 Min)	33.0 (36 Max/ 20 Min)	28	33.6 (at nominal)	--	--
Discharge Current [A]	10 (18 for 5s)	30	8.75	3.8 (at nominal)	--	--
Charge Current [A]	3	1.5 (4 in fast mode)	N/A	N/A	--	--
weight [kg]	1.4	0.39	2.6	0.3	0.9	1.98
Energy [kWh]	0.25	0.036	--	--	5.83	2.7
Volume [L]	0.87	0.17	7.8	0.58	2	4.6
Efficiency [%]	97%*	94%*	19%	50%	19%*	50%*
Usable Fuel Energy [Kwh]	0.207	0.033	--	--	1.11	1.35
Energy density [Wh/kg]	178	91	--	--	1231	682
Energy density [Wh/L]	288	133	--	--	554	293

*Usable energy depends on discharge rate, average power rate (113W) assumed for calculations. Fuel cell efficiency is calculated at nominal power.